Hybrid energy harvester based on piezoelectric and electromagnetic mechanisms

Bin Yang
Chengkuo Lee
National University of Singapore
Department of Electrical and Computer Engineering
4 Engineering Drive 3, Singapore 117576
elelc@nus.edu.sg

Wei Loon Kee
Siak Piang Lim
National University of Singapore
Department of Mechanical Engineering
9 Engineering Drive 1, Singapore 117576

Abstract. A novel hybrid energy harvester integrated with piezoelectric and electromagnetic energy harvesting mechanisms is investigated. It contains a piezoelectric cantilever of multilayer piezoelectric transducer (PZT) ceramics, permanent magnets, and substrate of two-layer coils. The effect of the relative position of coils and magnets on the PZT cantilever end and the poling direction of magnets on the output voltage of the energy harvester is explored. When the poling direction of magnets is normal to the coils plane, the coils yield the maximum output voltage, i.e., the type I and III devices. The maximum output voltage and power from the PZT cantilever of the type III device are 0.84 V and 176 μW under the vibrations of 2.5-g acceleration at 310 Hz, respectively. And the maximum output voltage and power from the coils are 0.78 mV and 0.19 μW under the same conditions, respectively. The power density from the type III device is derived as 790 $\mu W/cm^3$ from piezoelectric components and 0.85 $\mu W/cm^3$ from electromagnetic elements. © *2010 Society of Photo-Optical Instrumentation Engineers.* [DOI: 10.1117/1.3373516]

Subject terms: piezoelectric and electromagnetic mechanisms; energy harvester; power density.

Paper 09122RR received Jul. 15, 2009; revised manuscript received Dec. 15, 2009; accepted for publication Feb. 12, 2010; published online Apr. 2, 2010.

1 Introduction

The market for handheld electronics grows remarkably with diversified products ranging from mobile phones, PDAs and cameras to healthcare devices. Such market demand drives significant technology progress in development of low-power electronics and wireless communication technology. Harvesting energy from ambient vibrations to recharge a battery is a potential solution to realize handheld electronics with infinite lifespan, i.e., self-powered electronics. Typically, vibration-based energy harvesting devices use one of the following energy transduction mechanisms: electrostatic,[1,2] electromagnetic,[3,4] and piezoelectric[5–7] mechanisms. Recently, comprehensive review articles of the vibration-based energy harvesters in the microelectromechanical systems (MEMS) category have been reported.[8,9] Electrostatic energy harvesters employ either comb finger electrodes or parallel-plate electrodes as variable capacitors that are biased with external voltage sources and varied as a function of ambient vibrations.[2,10] This indicates that electrostatic energy harvesters are not passive devices. Electromagnetic energy harvesters collect the energy from the generated current from coils due to the variation of magnetic flux induced from the movement of a permanent magnet. Arnold[11] has reported the state-of-the-art and ongoing challenges in electromagnetic energy harvesters. This indicates that compact electromagnetic energy harvesters with size of several tens of millimeters can provide a few hundreds of microwatts. Such results promise a bright future of using microscale electromagnetic energy harvesters as an alternative power source for modern portable electronic devices. An electromagnetic energy harvester for intelligent sensor systems has been tested on a car engine.[12] In order to optimize the structural design and analysis of an electromagnetic energy harvester, an equivalent circuit model is used to analyze the system dynamics and the entire system in conjunction with nonlinear and/or active power electronic circuits.[13] Piezoelectric energy harvesters employ the mechanical strain of piezoelectric elements under loaded force due to direct piezoelectric effect. The main research interest in piezoelectric energy harvesters are improvement of power generation. Shu et al.[14] have studied the efficiency of energy conversion for a piezoelectric energy harvester by an analytical model. It is shown that the efficiency depends on the normalized resistance, the frequency ratio, the relative magnitudes of the electromechanical coupling coefficient, and the mechanical damping ratio. In order to increase the energy conversion efficiency, a piezoelectric energy harvester using air-spaced composite cantilevers for harvesting vibration energy has been proposed.[15] Ottman et al.[16,17] have developed an adaptive electric circuit model to optimize the energy transfer from the piezoelectric element to the energy-stored component.

Mitcheson et al. have compared the performance limits of the three MEMS energy harvesting mechanisms.[9,18] The resonant quality factor of electromagnetic energy harvesters is proportional to resonant frequency. In contrast, the resonant quality factor of piezoelectric energy harvesters is proportional to the square of frequency. Thus, the optimum output power of piezoelectric mechanisms becomes rapidly diminished with increased frequency. Within the high-frequency range, the degeneration rate of output power of piezoelectric mechanisms is more rapid than the one in the

electromagnetic case.[18] As a guideline, piezoelectric energy harvesters outperform electromagnetic energy harvesters at low frequency, and the electromagnetic mechanism is favorable in the high-frequency range. Piezoelectric energy harvesters usually produce high voltages and lower current. In comparison with piezoelectric energy harvesters, electromagnetic energy harvesters tend to produce relatively low AC voltage, and the voltage output is decreased when the size scales down.[19] A comparative study of electromagnetic and piezoelectric energy harvesters for portable devices has been presented.[20] It points out that piezoelectric energy harvesters present high power density and are more suitable for microsystem applications, while electromagnetic energy harvesters are good at applications of relatively large size. In order to overcome drawbacks of each individual type of the three energy harvesting mechanisms, a creative energy harvester is proposed to harness energy from typing motions on a computer keyboard by combining electromagnetic (in terms of typing speed and frequency) and piezoelectric (using typing force) mechanisms.[21] This energy harvester includes a 191-μm-thick layer of lead-zirconate-titanate piezoelectric transducer (PZT) ceramics coated with electrodes on double sides, and spiral coils of 13 turns with area of 1 cm^2 (i.e., 100-μm-wide aluminum coil electrode pattern with 100-μm spacing). The maximum power is about 40.8 μW from the PZT layer with a load resistance of 3 MΩ, while it is about 11.6 pW from the spiral coils with a 700 Ω load. This energy harvester shows the potential of providing enough power to recharge batteries while the keyboard is in use.

On the other hand, printed circuit board (PCB) technology has been proposed as a low-cost approach for making millimeter-scale MEMS devices such as scanning mirrors[22] and electromagnetic energy harvesters.[23] In view of the potential merits of integration of different mechanisms, a vibration-based energy harvester using a hybrid mechanism is proposed and studied. The proposed device consists of a multilayer PZT cantilever, a PCB substrate of two-layer coils, and magnets as seismic mass. The piezoelectric coupling model and magnetic simulation are used to validate the design concept and to conduct the optimization. As such, the output performance is optimized in terms of poling direction, moving direction of magnet, and location of coils.

Table 1 Structural parameters and material properties of magnet and PZT cantilever.

	Parameter	Description	Value
Material properties	E_1	Nd magnet Young's module	41.4e9 Pa
	ρ_1	Nd magnet density	7.4e3 kg/m^3
	v_1	Nd magnet Poisson	0.28
	m_1	Nd magnet mass	1.04e−4 kg
	ρ_2	PZT cantilever density	7.8e3 kg/m^3
	m_2	PZT cantilever mass	1.07e−3 kg
	e_{31}	Piezoelectric constant	5.8C m^{-2}
	$\varepsilon_{33}/\varepsilon_0$	Relative permittivity	560
	ε_0	Absolute permittivity	8.85e−12 F m^{-1}
Structural parameters	D	Diameter of single Nd magnet	3e−3 m
	T	Thickness of single Nd magnet	2e−3 m
	l_1	Free length of PZT cantilever	2.2e−2 m
	W_1	Width of PZT cantilever	9.6e−3 m
	t_1	Thickness of PZT cantilever	6.5e−4 m
	l_2	Length of single-layer coil area	1e−2 m
	W_2	Width of single-layer coil area	1e−2 m
	t_2	Thickness of coils substrate	5e−4 m

2 Design and Simulation

2.1 *Design of the Device*

Cofired multilayer piezoelectric cantilever elements from PIEZO Systems, Inc., are used in this work. This PZT cantilever is built up from a number of PZT layers, with each layer of 30-μm thickness and a few μm thick screen-printed electrodes between two layers of piezoelectric ceramic pattern. The length, width, and total thickness of the piezoelectric ceramic cantilever are 22 mm, 9.6 mm, and 0.65 mm, respectively. The properties of the PZT piezoelectric ceramic cantilever are listed in Table 1. As shown in Fig. 1, there are Nd permanent magnets fixed on the free tip of the cantilever as the proof mass. By doing so, the structural natural resonant frequency of the hybrid energy harvester is reduced for low-frequency vibration applications. The bilayer copper coils are placed near the magnets, which are made of thin fire-resistant 4 (FR4) substrates based on a standard PCB technology. Three types of hybrid energy harvesters are investigated in order to understand the influence of the relative position of PCB coils and magnets on output power, where PCB coils and magnets are manually assembled in the configurations as shown in Fig. 1. When the device is excited by external vibration sources, vibration kinetic energy can be converted electric energy via both electromagnetic and piezoelectric transduction mechanisms.

For the type I device in Fig. 1(a), the magnets are placed at the back side of the end of the PZT cantilever to tune the resonant frequency of the whole structure, while the magnetic coils are placed underneath the magnets. In contrast, the type II and III devices comprise the magnets arranged symmetrically on the double sides of the cantilever end with respect to the PCB coils, which are arranged vertically, as shown in Figs. 1(b) and 1(c), respectively. For type

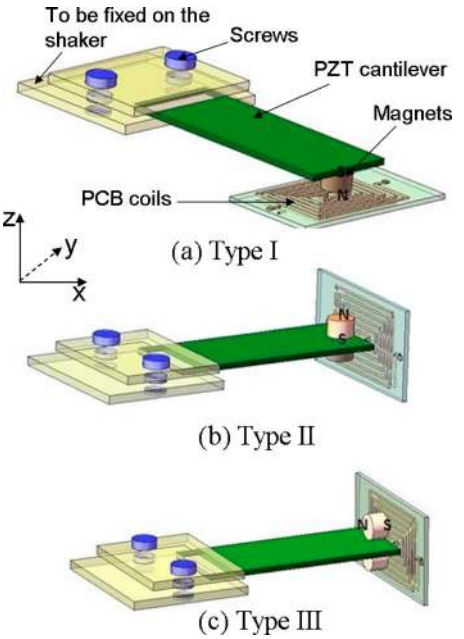

Fig. 1 Investigated movement directions of the magnet referring to the normal vector of the coil. (a) Type I: Magnets' poling direction along *z* axis; plane coils located in horizontal plane. (b) Type II: Magnets' poling direction along *z* axis; plane coils located in vertical plane. (c) Type III: Magnets' poling direction along *y* axis; plane coils located in vertical plane.

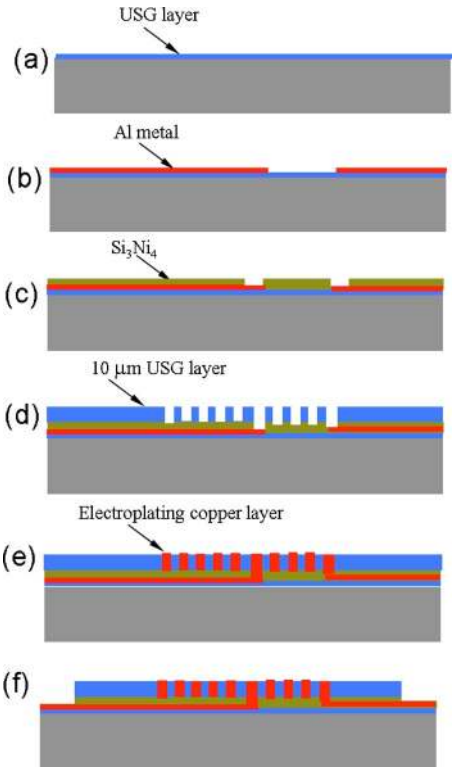

Fig. 2 Fabrication process flows of 3-D MEMS coils.

I and II devices, the poling direction of magnets is along the *z* direction, while the poling direction of magnets is along the *y* direction for type III devices.

In order to optimize the output power of electromagnetic mechanism, three-dimensional (3-D) integrated coils are designed and fabricated by MEMS technology. Figure 2 shows the fabrication process of 3-D coils. 2000 Å plasma-enhanced chemical vapor deposition (PECVD) undoped silicon glass (USG) is deposited as an insulating layer. Next, a 1-μm aluminum metal layer is sputtered to form the top and bottom electrodes for the wire bonding process. The other insulating layer of 2000 Å PECVD Si_3Ni_4 is deposited and patterned by using a reactive ion etching (RIE) process to expose connecting metal via, as shown in Fig. 2(c). In order to reduce the resistance of coils, the thickness of coils should be increased. A 10-μm-thick low-stress PECVD USG layer is deposited and patterned for the coils structure and exposed via, as shown in Fig. 2(d). The width and gap of coils are 3 μm and 5 μm, respectively. The dimension of the opening via is 10 μm $\times$ 10 μm. Then, a 250 Å/1500 Å Ta/Cu seed layer is sputtered on the USG layer, and 10-μm-thick copper coil is electroplated. After a chemical mechanical polishing (CMP) process, each turn of adjacent coil is separated. Last, the two wire bonding pads of coil electrodes are patterned, as shown Fig. 2(f). The SEM image of the final coil structure is shown in Fig. 3. Compared to PCB technology, the coil turns in the same coil area of 1 cm $\times$ 1 cm increase about 60 times.

2.2 *Electrical Power Output Model of Piezoelectric and Electromagnetic Mechanisms*

The inertial-based energy harvester is essentially a second-order, spring-mass system. When the external excitation is harmonic, a general model for the energy conversion from mechanical vibration energy to electrical energy is described by Eq. (1);

$$M\ddot{z} + (b_e + b_m)\dot{z} + kz = -M\ddot{y}, \tag{1}$$

where z is the relative displacement of the cantilever end, $\ddot{y}$ is the input vibration, M is a mechanical mass, b_e is the electrically induced damping coefficient, b_m is the mechanical damping coefficient, and k is the spring constant.

The direct piezoelectric effect of the piezoelectric element can be modeled by the linear constitutive equations, and its converse effect can be simulated by the electromechanical coupling coefficient. The electrical response of the piezoelectric material is dependent on the external mechanical loads, i.e., stress and strains, relative to a set of axes fixed in the material. For energy harvesting applications, the output voltage across and power dissipated in the loading resistance are two important parameters. The electrical model of the piezoelectric harvester can be represented by an RC equivalent circuit model,[21] and the output power given to the load is given by:

$$P_{pz} = \frac{V^2}{\left[1 + \left(\frac{R_{pz} + R_L}{\omega C_{pz} R_{pz} R_L}\right)^2\right] R_L}, \tag{2}$$

where V is the generated voltage from the piezoelectric cantilever, R_{pz} is the internal resistance, R_L is the loading resistance, ω is the vibration frequency, and C_{pz} is the internal capacitance.

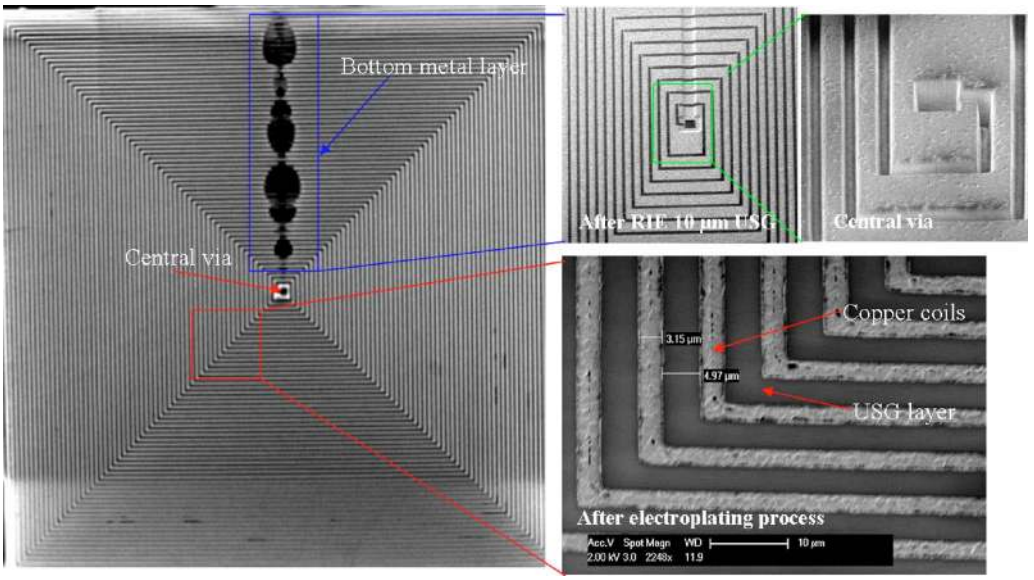

Fig. 3 SEM images of micromachined MEMS coils.

Based on Eq. (2), the output power can be optimized in terms of the internal resistance and capacitance of multilayer PZT, the loading resistance, and the vibration frequency. When the resonant frequency of the piezoelectric cantilever matches the ambient vibration frequency, the maximum output power is obtained. The n'th resonant frequency of a multilayer composite cantilever (clamped-free structure) with a large proof mass located at the free end tip is given by[24]:

$$f_n = \frac{\upsilon_n^2}{2\pi}\left[\frac{0.236EW_1}{(l_1 - D/2)^3(0.236mW_1l_1 + \Delta m)}\right]^{1/2}, \tag{3}$$

where υ_n is the n'th mode eigenvalue, E is a function of the Young's modulus of the two materials, W_1 is the width of the piezoelectric cantilever, l_1 is the length of the cantilever, D is the diameter of the magnet, m is the mass per unit length of the cantilever, and Δm is the proof mass of magnets added to the cantilever end. The targeted resonant frequency can be obtained by selecting the length and width of the PZT cantilever and the proof mass, i.e., the number of magnets assembled at the cantilever end. In this paper, the first resonant frequency of the multilayer PZT cantilever integrated with magnets is employed.

Assuming that an input displacement of $y(t) = Y\sin(\omega t)$ was applied to the inertial frame, the relative velocity of the cantilever at the steady state is given by:[3]

$$\dot{z}(t) = \frac{\left(\frac{\omega}{\omega_n}\right)^2 \omega Y}{\left\{\left[1 - \left(\frac{\omega}{\omega_n}\right)^2\right]^2 + \left(2\zeta\frac{\omega}{\omega_n}\right)^2\right\}^{1/2}} \cos(\omega t + \varphi), \tag{4}$$

where ω is the external vibration frequency, Y is the amplitude of vibration, φ is the phase angle, ω_n is the natural frequency of the system, and ζ is the total damping ratio of the system.

On the other hand, the generated voltage and power equations and the dynamic equations of motion are derived by an equivalent mass-spring-damper model for our designed large mass/coil type electromagnetic harvester.[25] The output power at steady state can be expressed by:

$$P_{em} = \frac{1}{2}\frac{(BL_P)^2 R_L}{(R_L + R_c)^2}\dot{z}^2, \tag{5}$$

where B is the magnetic flux density produced by the magnet and clearly decreases with the increase of gap between magnet and coil,[23] L_P is the practical coil length, R_C is the coil resistance, and R_L is the loading resistance.

Substituting Eq. (4) into Eq. (5),

$$P(t) = \frac{1}{2}\frac{(BL_P)^2 R_L}{(R_L + R_C)^2} \times \frac{\left(\frac{\omega}{\omega_n}\right)^4 \omega^2 Y^2}{\left[1 - \left(\frac{\omega}{\omega_n}\right)^2\right]^2 + \left(2\zeta\frac{\omega}{\omega_n}\right)^2} \cos^2(\omega t + \varphi). \tag{6}$$

Hence, the total power output of the device P_t is the sum of the power generated from the piezoelectric and electromagnetic harvesting mechanisms given by Eqs. (2) and (6), respectively,

$$P_t = P_{pz} + P_{em} = \frac{V^2}{\left[1 + \left(\frac{R_{pz} + R_L}{\omega C_{pz} R_{pz} R_L}\right)^2\right] R_L} + \frac{1}{2}\frac{(BL_P)^2 R_L}{(R_L + R_C)^2} \times \frac{\left(\frac{\omega}{\omega_n}\right)^4 \omega^2 Y^2}{\left[1 - \left(\frac{\omega}{\omega_n}\right)^2\right]^2 + \left(2\zeta\frac{\omega}{\omega_n}\right)^2} \cos^2(\omega t + \varphi). \tag{7}$$

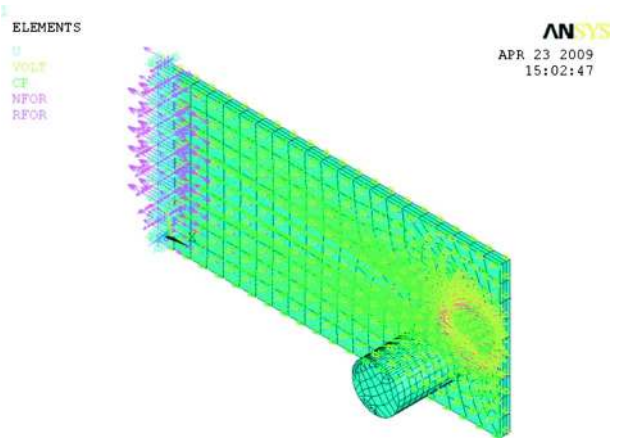

Fig. 4 Finite element model of different magnets using proof mass from type I.

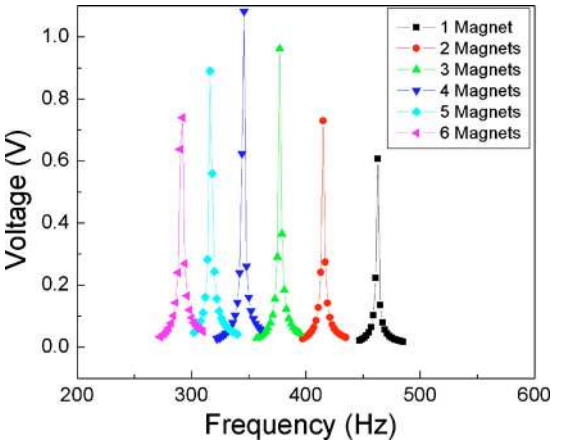

Fig. 5 Finite element simulated results of different magnets using proof masses from type I.

2.3 *Optimization of PZT Cantilevers with Different Numbers of Magnets*

Dynamic modeling of a piezoelectric cantilever assembled with magnets is conducted by using a finite element analysis (FEA) software ANSYS 10.0. The properties of PZT cantilever and magnet are listed in Table 1. Because the thickness of screen-printed laminated electrodes is very thin, its effect is neglected in the modeling. The three-dimensional piezoelectric coupled-field solid element of SOLID5 is used to simulate the cantilever, and SOLID95 is used for the magnets. For example, the finite element model with three magnets is shown in Fig. 4. The full-method harmonic analysis in ANSYS is employed to predict the output voltage of PZT cantilever with the different numbers magnets under the same loading case of 2.5-g acceleration, i.e., 3-μm vibration amplitudes at the resonance. The boundary condition is set by three steps: (1) constraining the nodal displacement in the x, y, and z directions at one end of the cantilever; (2) applying 0 V as the nodal electrical potential at the bottom electrode; and (3) coupling all nodal potential at the top electrode of the PZT cantilever. To optimize the output performance of PZT cantilevers with different numbers of magnets, a constant damping ratio of 0.2% is assumed, and the frequency is varied in the ranges of 445 to 485 Hz, 395 to 435 Hz, 355 to 395 Hz, 320 to 360 Hz, 300 to 340 Hz, and 270 to 310 Hz for the cantilever with a number of magnets from one to six, respectively. Twenty substeps within each scanned frequency range are recorded, i.e., the output voltage is recorded at every 2 Hz. Figure 5 gives the first resonant frequency and the resulting output voltage of PZT cantilevers integrated with magnets of various numbers as proof masses. This shows that the resonant frequency of each case is 463, 415, 377, 346, 316, and 292 Hz, respectively, and the output voltage of the PZT cantilever with four magnets exhibits maximum value of 1.082 V. This is owing to the nonlinear response of PZT under larger stress. Both the elastic compliance and damping coefficient increase as the stress is sufficiently large, while the piezoelectric constant decreases with increased stress.[26] For a damped harmonic oscillator, the damping coefficient c is given by:[27]

$$c = 2M\zeta\omega_1, \tag{8}$$

where M is the mass, ω_1 is natural angular frequency, and ζ is the damping ratio and is given by

$$\zeta = \frac{1}{2\pi n}\ln(x_1/x_2), \tag{9}$$

where x_1 is the amplitude at one point in time, and x_2 is a later amplitude measured after n periods of the sinusoidal response. The damping coefficient increases with the increasing of magnets numbers. Such facts result in low output voltage, low power conversion efficiency, and increased energy loss. Meanwhile, for a given input acceleration, the PZT cantilever generates larger strains in the case of more magnets numbers, i.e., 5 and 6 magnets. Thus, we conclude that the configuration of four magnets at the PZT cantilever end is the optimized structure of type I device.

2.4 *Magnetic Coils Design*

To understand how the magnetic flux affects surrounding coils with respect to the free-standing Nd magnet, the magnetic analysis in ANSYS is used to analyze it. The dimension of a cylinder magnet is 3 mm in diameter and 4 mm in length. Figure 6 shows the magnetic two-dimensional (2-D) flux lines distribution along the magnet cross-section plane (x-z plane). The simulation results show that the flux lines are mostly distributed in this area (x-y plane) of about 1 cm$\times$1 cm for the whole cylinder magnet. This indicates that the magnetic flux line distribution starts to decay drastically beyond this area. Thus, the copper coils are designed and made within this effective area. The structural parameters of coils in detail are also listed in Table 1.

3 Measurement and Discussion

Figure 7 shows the photographs of different prototypes, i.e., type I, type II, and type III. The PZT cantilever is fixed on top of the shaker through acrylic plates. As discussed in Ref. 23, a smaller gap contributes to an enlarged output voltage. In this paper, the gap between the magnets and coils is kept at 0.5 mm for all types of devices, and it is adjusted by a three-dimensional nano-position controller. In the experimental setup platform, the dynamic signal ana-

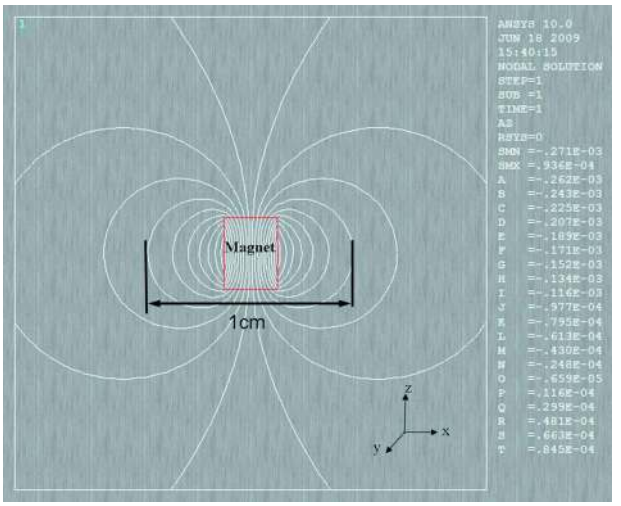

Fig. 6 Magnetic 2-D flux lines distribution by ANSYS.

Table 2 Comparison of the simulated and experimental data of resonant frequency and output voltage of PZT cantilevers.

	Performances			
	Resonant frequency (Hz)		Output voltage of PZT (V)	
Structures	FEM	Exp.	FEM	Exp.
1 magnet	463	459	0.606	0.523
2 magnets	415	407	0.729	0.593
3 magnets	377	383	0.962	0.642
4 magnets	346	350	1.082	0.66
5 magnets	316	330	0.89	0.537
6 magnets	292	310	0.74	0.359

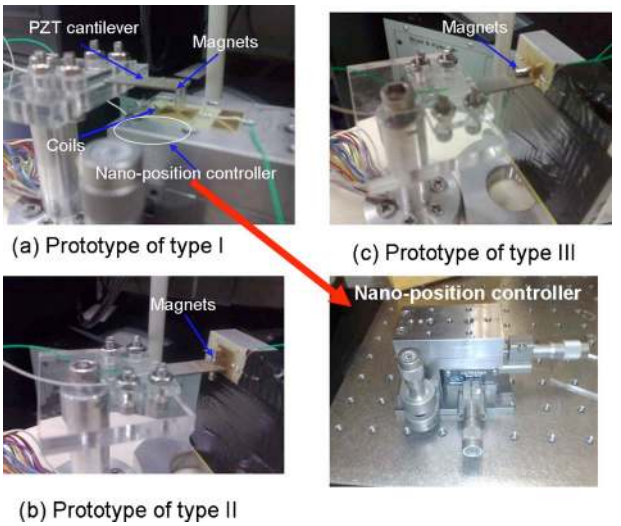

Fig. 7 Photograph of hybrid energy harvesting devices for different types: (a) type I; (b) type II; (c) type III.

lyzer is used to control the vibration amplitude of the shaker through power amplifier and the excited frequency and to record the output voltages from the PZT cantilever and coils.

Figures 8(a) and 8(b) show the open-circuit output voltages from the PZT cantilever and coils under the different numbers magnets at the acceleration level of 2.5 g, which are recorded by different channel of the dynamic signal analyzer, respectively. Based on Eq. (3), the resonant frequency decreases with the increased proof mass, i.e., number of magnets. When four magnets are added on the cantilever end, the output voltages of PZT cantilever and coils are obtained as maximum values of 0.66 V and 0.75 mV for the PZT cantilever and coils, respectively. Table 2 shows the comparison of FEA and experimental data regarding to resonant frequency and output voltage of the PZT cantilever. There is good agreement between the simulation and experimental results. The damping coefficient increases with proof mass from Eq. (8). Thus, in the case of

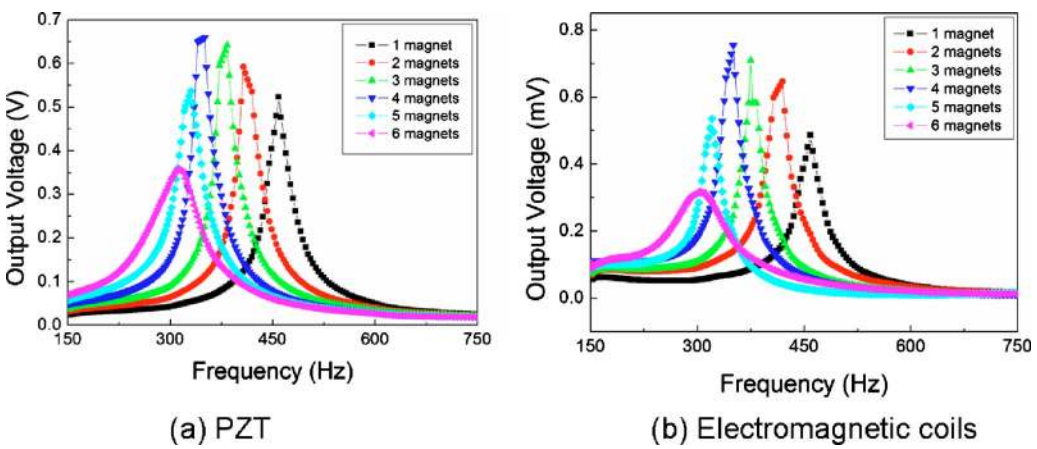

Fig. 8 Measured open-circuit output voltages (V_{rms}) versus excited frequency from type I: (a) generated voltage from piezoelectric cantilever; (b) generated voltage from electromagnetic coils.

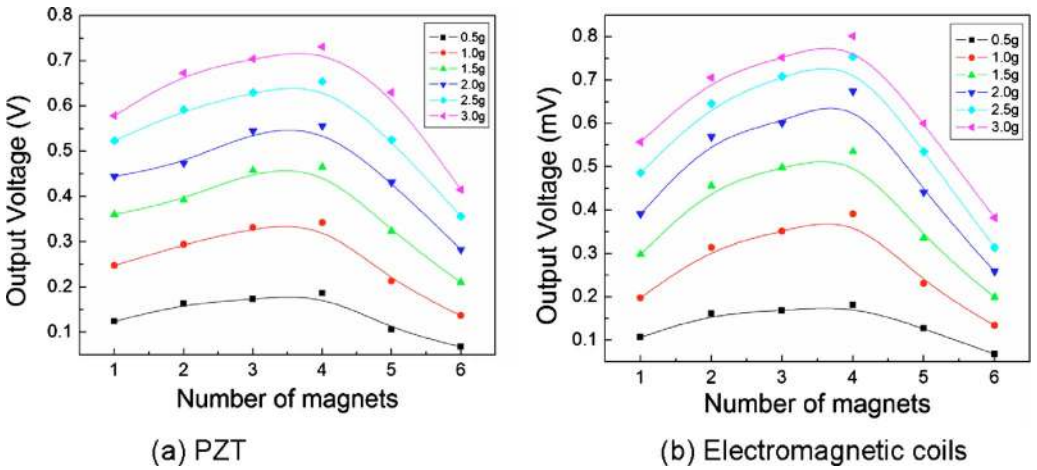

Fig. 9 Measured open-circuit output voltages (V_{rms}) versus numbers of magnets under different loading acceleration from type I: (a) generated voltage from piezoelectric cantilever; (b) generated voltage from electromagnetic coils.

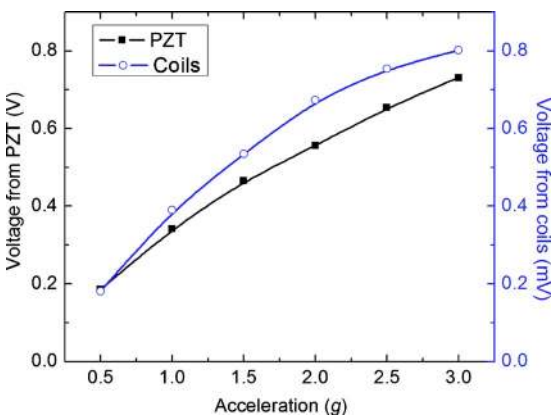

Fig. 10 Measured open-circuit output voltages (V_{rms}) from piezoelectric and electromagnetic mechanism at different accelerations.

more magnets, the output voltages of experiments are smaller than simulation results due to larger damping ratio in the experiments compared to the constant damping ratio of 0.2% and the piezoelectric constant (listed in Table 1) used in the simulations.

Figures 9(a) and 9(b) show the output voltage of PZT cantilever and coils versus the magnet numbers under vibrations of different accelerations from 0.5 g to 3.0 g, respectively. As we already observed in Fig. 8, the maximum output is always observed in a type I device of four magnets for all the measured curves under different accelerations in Fig. 9. The output voltage increases gradually with the increment of the accelerations. This is owing to the increase of vibration amplitude under larger acceleration based on Eq. (4). By recording the peak values of output voltage for the cases of four magnets in Fig. 9, fitting curves of measured output voltage data versus vibrations of various accelerations are shown in Fig. 10. The observed output voltage increases more and more slowly with the increase of acceleration, because the damping ratio slightly

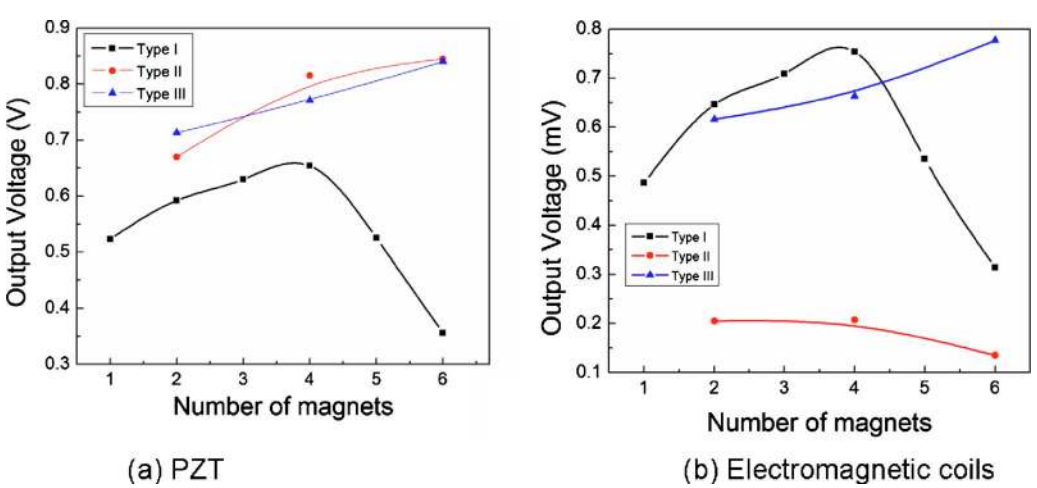

Fig. 11 Measured open-circuit output voltages (V_{rms}) versus numbers of magnets in the cases of type I, type II, and type III: (a) generated voltage from piezoelectric cantilever; (b) generated voltage from electromagnetic coils.

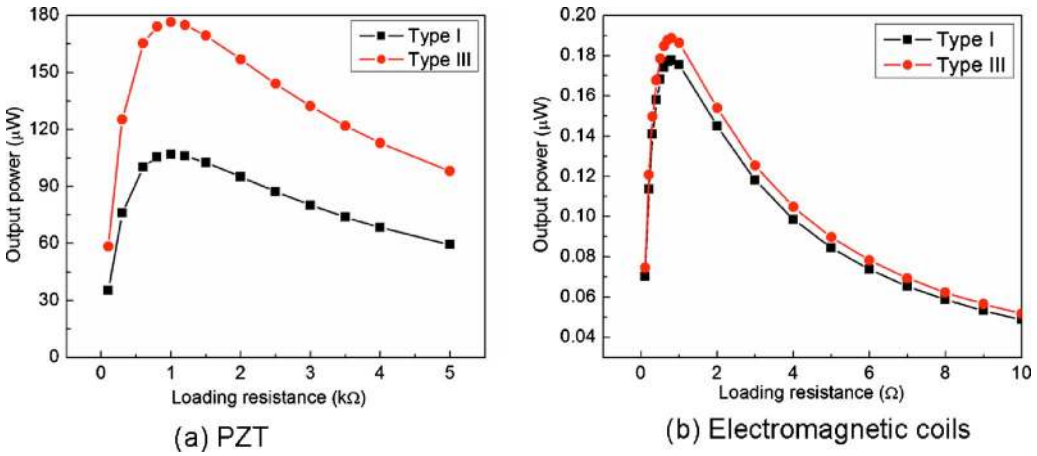

Fig. 12 Output power versus loading resistance: (a) generated power from piezoelectric cantilever; (b) generated power from electromagnetic coils.

increases as the acceleration increases due to the nonlinear response of PZT cantilever under larger stress.[24,28]

Figures 11(a) and 11(b) show the output voltages of the PZT cantilever and coils under the acceleration of 2.5 g as a function of magnet numbers for devices of type I, II, and III, respectively. Magnets are distributed symmetrically on the double sides of the PZT cantilever end for types II and III, which results in almost the same output voltage from piezoelectric mechanism. But the output voltage level is larger than that of type I, especially for the case of more than four magnets, as shown in Fig. 11(a). For types II and III devices, the PCB coils substrate is placed vertically against to the end of cantilever, and this configuration results in lower damping ratio for a given input acceleration. For the electromagnetic energy harvesting mechanism, the magnetic flux change is a key impact factor according to Eq. (5). The magnetic flux is also determined by the relative location between the poling direction of magnets and coils plane. When the poling direction of magnets is normal to the coils plane, e.g., the cases of types I and III, the output voltage from coils is much higher than that of the type II device, i.e., the poling direction of magnets parallel to the coils plane. Thus, the output voltage of type I devices ranges from 0.5 mV to 0.74 mV for magnets of 1 to 4, and the output voltage of 0.6 mV to 0.77 mV is derived for type III devices of 2, 4, and 6 magnets. In contrast, the output voltage of 0.2 mV to 0.13 mV is derived for type II devices of 2, 4, and 6 magnets, as shown in Fig. 11(b). Based on Eqs. (4) and (5), apart from the magnetic flux change, the relative motion velocity between magnets and coils is the other key impact factor. The relative moving displacement of the PZT cantilever end for type I device decreases when the attached magnet number is more than four. Hence, the piezoelectric output voltage and coils output voltage for type I device decrease as the magnet number is larger than 4, as shown in Figs. 11(a) and 11(b), due to the fact that the relative displacement is reduced. Meanwhile, as we discussed in Fig. 5, the elastic compliance and damping coefficient increase when the stress is sufficiently large, and the piezoelectric constant decreases with increased stress. This part of the effect also contributes to the reduced value of the piezoelectric output voltage for type I device with the number of magnets more than four in Fig. 11(a).

The internal resistance of the PZT cantilever measured by impedance analyzer is about 1 kΩ, and the internal resistance of two-layer copper coils is 0.8 Ω. The output power of the PZT cantilever and coils can be derived by the following equation:

$$P = \left(\frac{V}{R_S + R_L}\right)^2 R_L, \tag{10}$$

where V is the measured output voltage, R_S is the internal resistance of PZT cantilever or PCB coils, and R_L is loading resistance.

Figures 12(a) and 12(b) show the output power of the PZT cantilever and PCB coils under different loading resistance for type I and III devices, respectively. When the loading resistance matched with the internal resistance of PZT cantilever, the maximum piezoelectric output power of type I and III is 107 μW and 176 μW under the vibrations of 2.5-g acceleration at 350 Hz and 310 Hz, respectively. In addition, the maximum output power of type I and III from electromagnetic mechanism is 0.18 μW and 0.19 μW, respectively, when the loading resistance is matched with the internal resistance of coils. To evaluate the power density, we derived the overall volume of the energy harvester including PZT cantilever and magnets. Thus, the volume of the type I device with four magnets and the type III device with six magnets is calculated as 194 mm^3 and 222 mm^3, respectively. The power densities of piezoelectric and electromagnetic mechanisms for type I and type III devices are derived as 550 $\mu W/cm^3$ and 0.93 $\mu W/cm^3$, and 790 $\mu W/cm^3$ and 0.85 $\mu W/cm^3$, respectively. The operation frequency, whole structural volume, and output performance of other published piezoelectric energy harvesters are listed in Table 3 for comparison. This indicates that the power density of piezoelectric mechanism reported in this paper demonstrates comparable performance.

Table 3 Performance comparison among published piezoelectric harvesters and our device.

Author	Frequency (Hz)	Power (μW)	Volume (mm^3)	Power density (μW cm^{-3})
Ghynne-Jones et al. (Ref. 29)	80.1	2.1	125	17
Roundy et al. (Ref. 10)	210	375	1000	375
Sodano et al. (Ref. 30)	30	11.9	240	50
Bayrashev et al. (Ref. 31)	5	80	2185	37
Shen et al. (Ref. 32)	183.8	0.32	0.769	416
Marzencki et al. (Ref. 33)	204	0.038	3.8[a]	10
Yang et al. (in this research)	310	176	222	790

[a]Estimated from data in reference.

Because the induced electromotive force voltage is proportional to the coil turns, i.e., the practical coil length based on Eq. (5), the output voltage from 3-D MEMS coils is about 48.36 mV under the vibrations of 2.5-g acceleration. Based on Eqs. (5) and (6), the output power is also the function of internal resistance apart from the induced electromotive force voltage. But the internal resistance of 3-D MEMS coils also increases due to the increase of coils length, while its value is about 710 Ω. The generated power increases to about 320% (from 0.19 μW to 0.8 μW) due to the increased turns by using 3-D MEMS coils.

4 Conclusion

This paper describes a novel hybrid energy harvester for collecting vibration energy based on piezoelectric and electromagnetic mechanisms. A PZT piezoelectric cantilever integrated with permanent magnets at the cantilever end is assembled with a PCB substrate of two-layer coils. The number of magnets, i.e., different value of added mass, the relative position of coils and magnets, and the poling direction of placed magnets are critical to the output voltage and power of energy harvester. The optimization simulation and experiments have been performed. For the type I device, the output voltages of PZT cantilever with four magnets and coils obtain the maximum level of 0.66 V and 0.75 mV under the vibration of 2.5-g acceleration. When the poling direction of magnets is normal to the coils plane, the output voltage from coils is in the optimal condition, as observed in type I and type III devices. The output power of the PZT cantilever and coils is measured as high as 176 μW and 0.19 μW for a type III device with six magnets under the vibrations of 2.5-g acceleration at 310 Hz. Among all the tested configurations, type I devices show maximum output power of 107 μW in the case of four magnets under the vibrations of 2.5-g acceleration at 350 Hz. The major advantages of our device are low cost and capability of harvesting energy by both piezoelectric and electromagnetic mechanisms.

Acknowledgments

The authors thank the testing support from Institute of Microelectronics (IME), A*STAR. This research is partially funded by A*STAR HOME 2015 National Research Programme (SERC Grant No. 0621150043) and by the National University of Singapore under Grant No. R-263-000-475-112.

References

1. P. D. Mitcheson, P. Miao, B. H. Stark, E. M. Yeatman, A. S. Holmes, and T. C. Green, "MEMS electrostatic micropower generator for low frequency operation," *Sens. Actuators, A* **115**, 523–529 (2004).
2. S. Menigner, J. O. Mur-Miranda, R. Amirtharajah, A. P. Chandrakasan, and J. H. Lang, "Vibration-to-electric energy conversion," *IEEE Trans. Very Large Scale Integr. (VLSI) Syst.* **9**, 64–76 (2001).
3. I. Sari, T. Balkan, and H. Kulah, "A electromagnetic micro power generator for wideband environmental vibrations," *Sens. Actuators, A* **145**, 405–413 (2008).
4. S. P. Beeby, R. N. Torah, M. J. Tudor, P. Glynne-Jones, T. O'Donnell, C. R. Saha, and S. Roy, "A micro electromagnetic generator for vibration energy harvesting," *J. Micromech. Microeng.* **17**, 1257–1265 (2007).
5. F. Lu, H. P. Lee, and S. P. Lim, "Modeling and analysis of micro piezoelectric power generators for micro-electromechanical-systems applications," *Smart Mater. Struct.* **13**, 57–63 (2004).
6. S. Roundy and P. K. Wright, "A piezoelectric vibration based generator for wireless electronics," *Smart Mater. Struct.* **13**, 1131–1142 (2004).
7. J. Q. Liu, H. B. Fang, Z. Y. Xu, X. H. Mao, X. C. Shen, D. Chen, H. Liao, and B. C. Cai, "A MEMS-based piezoelectric power generator array for vibration energy harvesting," *Microelectron. J.* **39**, 802–806 (2008).
8. S. P. Beeby, M. J. Tudor, and N. M. White, "Energy harvesting vibration sources for microsystems applications," *Meas. Sci. Technol.* **17**, R175–R195 (2006).
9. P. D. Mitcheson, E. M. Yeatman, G. K. Rao, A. S. Holmes, and T. C. Green, "Energy harvesting from human and machine motion for wireless electronic devices," *Proc. IEEE* **96**, 1457–1486 (2008).
10. S. Roundy, P. K. Wright, and J. Rabaey, "A study of low level vibrations as a power source for wireless sensor nodes," *Comput. Commun.* **26**, 1131–1144 (2003).
11. D. P. Arnold, "Review of microscale magnetic power generation," *IEEE Trans. Magn.* **43**, 3940–3951 (2007).
12. P. Glynne-Jones, M. J. Tudor, S. P. Beeby, and N. M. White, "An electromagnetic, vibration-powered generated for intelligent sensor systems," *Sens. Actuators, A* **110**, 344–349 (2004).
13. S. Cheng, N. Wang, and D. P. Arnold, "Modeling of magnetic vibrational energy harvesters using equivalent circuit representations," *J. Micromech. Microeng.* **17**, 2328–2335 (2007).
14. Y. C. Shu and I. C. Lien, "Efficiency of energy conversion for a piezoelectric power harvesting system," *J. Micromech. Microeng.* **16**, 2429–2438 (2006).
15. Z. Wang and Y. Xu, "Vibration energy harvesting device based on air-spaced piezoelectric cantilevers," *Appl. Phys. Lett.* **90**, 263512 (2007).
16. G. K. Ottman, H. F. Hofmann, A. C. Bhatt, and G. A. Lesieutre, "Adaptive piezoelectric energy harvesting circuit for wireless remote power supply," *IEEE Trans. Power Electron.* **17**, 669–676 (2002).
17. G. K. Ottman, H. F. Hofmann, and G. A. Lesieutre, "Optimized piezoelectric energy harvesting circuit using step-down converter in discontinuous conduction mode," *IEEE Trans. Power Electron.* **18**, 696–703 (2003).
18. P. D. Mitcheson, E. K. Reilly, T. Toh, P. K. Wright, E. M. Yeatman, "Performance limits of the three MEMS inertial energy generator transduction types," *J. Micromech. Microeng.* **17**, S211–216 (2007).
19. S. Roundy, "On the effectiveness of vibration-based energy harvesting," *J. Intell. Mater. Syst. Struct.* **16**, 809–823 (2005).
20. G. Poulin, E. Sarraute, and F. Costa, "Generation of electrical energy for portable devices: comparative study of an electromagnetic and a piezoelectric system," *Sens. Actuators, A* **116**, 461–471 (2004).
21. T. Wacharasindhu and J. W. Kwon, "A micromachined energy harvester from a keyboard using combined electromagnetic and piezoelectric conversion," *J. Micromech. Microeng.* **18**, 104016 (2008).
22. A. D. Yalcinkaya, O. Ergeneman, and H. Urey, "Polymer magnetic scanners for bar code applications," *Sens. Actuators, A* **17**, 236–243 (2007).

23. B. Yang, C. Lee, W. F. Xiang, J. Xie, H. He, R. K. Kotlanka, S. P. Low, and H. H. Feng, "Electromagnetic energy harvesting from vibrations of multiple frequencies," *J. Micromech. Microeng.* **19**, 035001 (2009).
24. D. N. Shen, J. H. Park, J. Ajitsaria, S. Y. Choe, H. C. Wikle III, and D. J. Kim, "The design, fabrication and evaluation of a MEMS PZT cantilever with integrated Si proof mass for vibration energy harvesting," *J. Micromech. Microeng.* **18**, 055017 (2008).
25. H. Kulah and K. Najafi, "Energy scavenging from low-frequency vibrations by using frequency up-conversion for wireless sensor applications," *IEEE Sens. J.* **8**, 261–268 (2008).
26. ANSI/IEEE "IEEE standard on piezoelectricity std," pp. 176–1987 (1987).
27. S. J. Roundy, "Energy scavenging for wireless sensor nodes with a focus on vibration to electricity conversion," PhD Thesis, Univ. of California, Berkeley (2003).
28. L. Q. Yao, J. G. Zhang, L. Lu, and M. O. Lai, "Nonlinear dynamic characteristics of piezoelectric bending actuators under strong applied electric field," *J. Microelectromech. Syst.* **13**, 645–652 (2004).
29. P. Glynne-Jones, S. P. Beeby, and N. M. White, "Towards a piezoelectric vibration powered microgenerator," *IEE Proc.: Sci., Meas. Technol.* **148**, 68–72 (2001).
30. H. A. Sodano, G. Park, and D. J. Inman, "Estimation of electric charge output for piezoelectric energy harvesting," *Strain* **40**, 49–58 (2004).
31. A. Bayrashev, W. P. Robbins, and B. Ziaie, "Low frequency wireless powering of microsystrems using piezoelectric-magnetostrictive laminate composites," *Sens. Actuators, A* **114**, 244–249 (2004).
32. D. N. Shen, J. H. Park, J. H. Noh, S. Y. Choe, S. H. Kim, H. C. Wikle III, and D. J. Kim, "Micromachined PZT cantilever based on SOI structure for low frequency vibration energy harvesting," *Sens. Actuators, A* **154**, 103–108 (2009).
33. M. Marzencki, B. Charlot, S. Basrour, M. Colin, and L. Valbin, "Design and fabrication of piezoelectric micro power generators for autonomous microsystems," in *Symp. on Design Testing Integration and Packaging of MEMS/MOEMS (DTIP7'05)*, B. Courtois, Ed., Montreux, Switzerland, pp. 299–302, Springer, Netherlands (2005).

Bin Yang received a BS degree in materials science from Anhui University of Technology and Science, China, in 2000. He received his MS degree in materials science from Jilin University in 2003 and PhD degree in electronic science and technology from Shanghai Jiao Tong University, China, in 2006. From 2006 to 2007, he was employed as a research fellow at the Department of Mechanical Engineering, National University of Singapore. From 2007 to 2009, he was a senior research engineer at the Institute of Microelectronics (IME). He is currently a research fellow at the Department of Electrical and Computer Engineering, National University of Singapore. His research interests include energy harvesters, optical MEMS, piezoelectric actuators, and sensors.

Chengkuo Lee received an MS degree in materials science and engineering from National Tsing Hua University, Hsinchu, Taiwan, in 1991. He also received an MS degree in industrial and system engineering from Rutgers University, New Brunswick, NJ, in 1993. He received a PhD degree in precision engineering from the University of Tokyo, Japan, in 1996. Since 1997, he has been at the Metrodyne Microsystem Corporation, Hsinchu, Taiwan. He was an adjunct assistant professor in the Electrophysics Department of National Chiao Tung University in 1998. Currently, he is an assistant professor in the Department of Electrical and Computer Engineering of the National University of Singapore and a senior member of the technical staff at the Institute of Microelectronics, Singapore. He has contributed more than 120 international conference papers and extended abstracts, 65 peer-reviewed international journal articles, and 8 U.S. patents in the MEMS, nanophotonics, and nanotechnology fields. He is a member of IEEE, MRS, and IEE Japan.

Biographies and photographs of the other authors are not available.